Graphene Pyramids

DOI: 10.1002/anie.201306317

Large Hexagonal Bi- and Trilayer Graphene Single Crystals with Varied Interlayer Rotations**

Zheng Yan, Yuanyue Liu, Long Ju, Zhiwei Peng, Jian Lin, Gunuk Wang, Haiqing Zhou, Changsheng Xiang, E. L. G. Samuel, Carter Kittrell, Vasilii I. Artyukhov, Feng Wang, Boris I. Yakobson,* and James M. Tour**

Abstract: *Bi- and trilayer graphene have attracted intensive interest due to their rich electronic and optical properties, which are dependent on interlayer rotations. However, the synthesis of high-quality large-size bi- and trilayer graphene single crystals still remains a challenge. Here, the synthesis of 100 μm pyramid-like hexagonal bi- and trilayer graphene single-crystal domains on Cu foils using chemical vapor deposition is reported. The as-produced graphene domains show almost exclusively either 0° or 30° interlayer rotations. Raman spectroscopy, transmission electron microscopy, and Fourier-transformed infrared spectroscopy were used to demonstrate that bilayer graphene domains with 0° interlayer stacking angles were Bernal stacked. Based on first-principle calculations, it is proposed that rotations originate from the graphene nucleation at the Cu step, which explains the origin of the interlayer rotations and agrees well with the experimental observations.*

Graphene, a two-dimensional sp^2-bonded carbon material, has attracted enormous attention due to its excellent electrical, optical and mechanical properties.[1] To date, the best-quality graphene is mechanically exfoliated from graphite though limited to small flakes and low yields, whereas large-area graphene grown on transition metals by chemical vapor deposition (CVD)[2] has produced polycrystalline structures with reduced electrical and mechanical properties.[3] Recent advancements in CVD techniques have enabled the fabrication of large-size and high-quality single-crystal monolayer graphene.[4] However, monolayer graphene has zero band gap, limiting its potential applications.[1] In contrast, bi- and trilayer graphene have rich electronic and optical properties that are dependent on their interlayer stacking orders, opening broad applications in nanoelectronics and optics.[1c,5] Therefore, CVD synthesis of large bi- and trilayer graphene single crystals with well-defined interlayer stacking that can be isolated from their growing substrates would provide a material with both fundamental interests and practical applications. In addition, it is unclear how the few-layer graphene single crystals are grown, and what determines the interlayer stacking. A combination of experimental and theoretical studies would offer useful guidance towards controlled synthesis of nanocarbon materials.

We report here the synthesis of about 100 μm pyramid-like bi- and trilayer graphene domains with hexagonal shapes on Cu foils. The as-made graphene domains can be isolated from the Cu surfaces and transferred onto silica wafers or trench-patterned silica wafers to suspend them without introducing damages or folds. This process has great potential for studying stacking-dependent electronics and optics in these graphene domains. Moreover, we found that the as-produced graphene domains show almost exclusively either 0° or 30° interlayer rotations. Raman spectroscopy, transmission electron microscopy (TEM), and Fourier-transformed infrared spectroscopy (FT-IR) with synchrotron radiation were used to demonstrate that bilayer graphene domains with 0° interlayer stacking angles were Bernal stacked. The 0° Bernal stacking is known to dominate in graphite,[6] but the 30° interlayer rotation is anomalous as it is incommensurate stacking.[7] Based on first-principle calculations, we propose that rotations originate from the graphene nucleation at the Cu step, which explains the origin of the interlayer rotations and agrees well with the experimental observations.

The fabrication of single-crystal hexagonal bi- and trilayer graphene domains was achieved in one batch on electrochemically polished and high-pressure annealed Cu foils using a double-annealing process (Figure 1a). The detailed growth procedures are described in the Supporting Information. After growth, graphene domains were transferred onto SiO_2 (100 nm)/Si substrates[4a] for optical characterizations, which permit the direct visualization of shapes and thicknesses of the as-produced graphene domains. Figure 1b–g and Figure S1 provide representative optical images of as-produced graphene domains on SiO_2/Si wafers. From these optical

[*] Z. Yan,[+] Z. Peng, Dr. G. Wang, Dr. H. Zhou, C. Xiang, E. L. G. Samuel, C. Kittrell, Prof. J. M. Tour
Department of Chemistry, Rice University
Houston, TX 77005 (USA)
E-mail: tour@rice.edu
Y. Liu,[+] Dr. J. Lin, Dr. V. I. Artyukhov, Prof. B. I. Yakobson, Prof. J. M. Tour
Department of Mechanical Engineering and Materials Science and
The Smalley Institute for Nanoscale Science and Technology
Rice University, Houston, TX 77005 (USA)
E-mail: biy@rice.edu
L. Ju, Prof. F. Wang
Department of Physics, University of California at Berkeley
Berkeley, CA 94720 (USA)
E-mail: fengwang76@berkeley.edu
[+] These authors contributed equally to this work.

[**] The ONR MURI program (grant numbers 00006766 and N00014-09-1-1066) and AFOSR MURI (grant number FA9550-12-1-0035) provided funding. We acknowledge M. Martin and H. Bechtel at the Lawrence Berkeley National Laboratory for help on the FTIR measurement.

Supporting information for this article is available on the WWW under http://dx.doi.org/10.1002/anie.201306317.

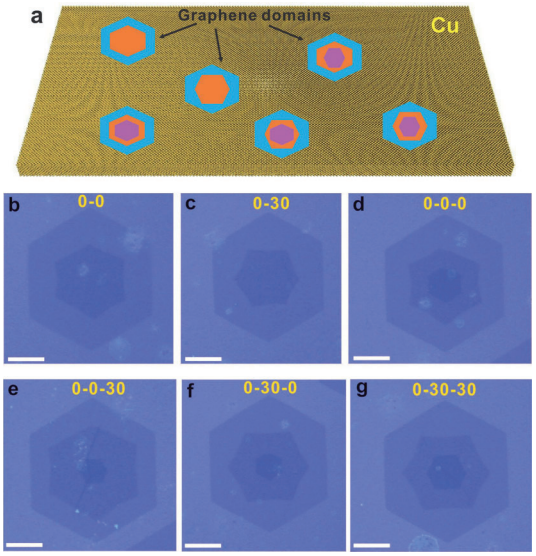

Figure 1. a) Bi- and trilayer graphene domains synthesized on Cu. b–g) Representative optical images of large pyramid-like bi- and trilayer graphene domains on SiO_2 (100 nm)/Si substrates. The scale bars in b–g are 30 μm.

images, we can see that individual single-crystal graphene domains could be completely isolated from growing substrates and transferred on silica wafers without inducing any damages or folds, indicating great potential for studying their stacking-order-dependent electronic and optical properties. In the same graphene domains, mono-, bi- or trilayer regions show hexagonal shapes and could be diffentiated by optical microscopy, with lateral distances of monolayer hexagons at about 100 μm. Interestingly, though, in the same graphene domain, mono-, bi- or trilayer hexagons show decreased lateral sizes, they share almost the same hexagonal center, meaning they nucleated from the same active sites at different times or at different growth rates. Additionally, according to recent research, the secondary graphene layer should nucleate and grow underneath the first graphene layer.[8]

More interestingly, in contrast to graphite where Bernal stacking dominates,[6] the as-produced few-layer graphene domains on the pretreated Cu demonstrated both 0° and 30° rotation preference (Figure 1 and Figure S1). In this research, 90 few-layer graphene domains were investigated, with about 48% of 0° interlayer stacking, about 46% of 30° interlayer stacking and only about 6% of randomly twisted stacking. Two types of bilayer graphene domains and four types of trilayer graphene domains were synthesized, according to their different interlayer stacking orders. Assuming orientation angles of monolayer hexagons in all graphene domains are 0° and, depending on different interlayer stacking orders, the as-made bi- and trilayer graphene domains are named as follows: 0-0 bilayer, 0-30 bilayer, 0-0-0 trilayer, 0-0-30 trilayer, 0-30-0 trilayer, and 0-30-30 trilayer (Figure 1 b–g, respectively). In the same growth batch, through the investigation of 115 graphene domains, 50% are bilayer domains, 30% are trilayer domains, and 20% are monolayer and tetralayer domains, with domain sizes of monolayer hexagons ranging from 70 to 130 μm. All of the different graphene domains can be transferred onto the same target substrate, such as a silica wafer, for further optical and electronic investigations. Moreover, Figures S2-4 show that bi- and trilayer graphene domains could be transferred onto trench-patterned silica wafers, indicating potentials of studying their stacking-order-dependent ballistic transport behaviors and thermal conduction in the future.[9]

As a demonstration, in this research, we investigated two types of bilayer graphene domains, 0-0 bilayer and 0-30 bilayer, using Raman spectroscopy, TEM, and FT-IR with synchrotron radiation (Figure 2). Figure 2a is a typical optical image of 0-0 bilayer graphene domains, showing concentric mono- and bilayer hexagons with 0° interlayer stacking orientation. Raman spectroscopy, a powerful tool to determine thickness and quality of graphene,[10] was first used to investigate this graphene domain. More than ten points were characterized by Raman spectroscopy on this 0-0 bilayer graphene domain, and the typical data of the monolayer region (point A) and the bilayer region (point B) are shown in Figure 2b. Figure 2b demonstrates that point A has the typical Raman spectrum of monolayer graphene, with an intensity ratio of G to 2D less than 0.5 and the full width at half maximum (fwhm) of the 2D peak at 30 cm^{-1}.[10] In contrast, the Raman spectrum of point B has an intensity ratio of G to 2D of about 1 and a fwhm of the 2D peak of 50 cm^{-1}.

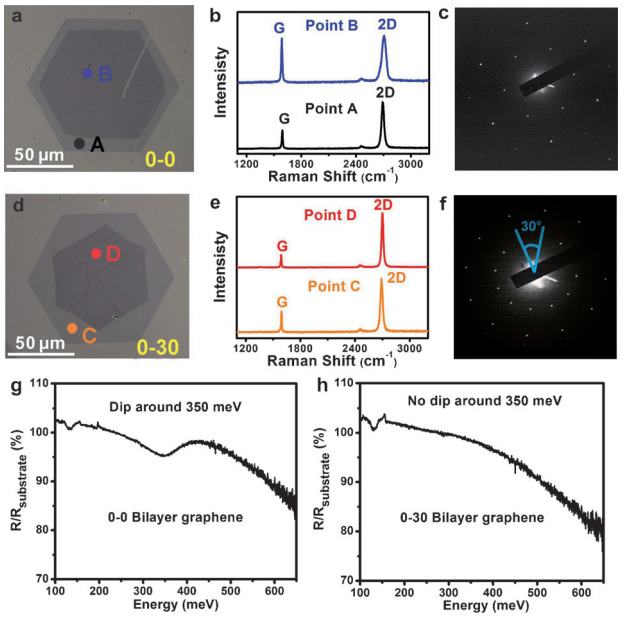

Figure 2. a) One typical optical image of 0–0 bilayer graphene domains. b) Raman spectra recorded from points A and B in panel (a). c) A typical SAED pattern taken from the bilayer region of 0–0 bilayer graphene domains, showing only one set of diffraction patterns. d) One typical optical image of 0-30 bilayer graphene domains. e) Raman spectra recorded from points C and D in panel (d). f) A typical SAED pattern taken from the bilayer region of 0-30 bilayer graphene domains, showing a 30° rotation between the two stacking layers. g) A representative reflection spectrum by FT-IR spectroscopy recorded from the bilayer region of 0–0 bilayer graphene domains, showing a dip around 350 meV. h) A representative reflection spectrum by FT-IR spectroscopy recorded from the bilayer region of 0-30 bilayer graphene domains.

Furthermore, the 2D peak (Figure S5) displays an asymmetric line shape and can be well-fitted by four components, each with fwhm of 30 cm^{-1}. These data indicate that the 0-0 bilayer graphene domain is Bernal-stacked.[10] Meanwhile, no obvious D peaks were detected in either the mono- or bilayer regions of 0-0 bilayer graphene domains, indicating the presence of few sp^3 carbon atoms or defects.[10] Selected area electron diffraction (SAED) patterns corroborate the stacking order in 0-0 bilayer graphene domains. Figure 2c shows only one set of SAED patterns in the bilayer region of 0-0 bilayer graphene domains. As shown in Figure S6, the (1-210) intensity was about three times stronger than the (1-100), further demonstrating the Bernal-stacked order of 0-0 bilayer graphene domains.[11]

Figure 2d is a typical optical image of 0-30 bilayer graphene domains, showing concentric mono- and bilayer hexagons with 30° stacking orientation. The Raman spectra in Figure 2e show that both the monolayer region (point C) and the bilayer region (point D) demonstrate typical Raman spectrum of monolayer graphene, meaning that the top layer and the bottom layer are fully decoupled in the 0-30 bilayer graphene domains.[12] Additionally, no D peaks were observed in Figure 2e, demonstrating the high-quality of as-produced 0-30 bilayer graphene domains.[10] Two sets of SAED patterns (Figure 2f and Figure S7) were observed in the bilayer region of 0-30 bilayer graphene domains. Interestingly, even in the same SAED, the measured twist angles differ from 26° to 34° (Figure S7), which were rounded to 30° in this research. This distortion could arise from the corrugated structures of suspended graphene that occur in large part due to the transfer process to the TEM grid.[13] In addition, the bilayer nature of as-made 0-0 and 0-30 graphene domains were further confirmed by the high-resolution TEM images of their exposed edges (Figure S8).

The stacking order can be further confirmed by FT-IR spectroscopy with synchrotron radiation. As shown in Figure 2g, 0-0 bilayer graphene shows a dip at 350 meV in the reflection spectrum. This can be ascribed to the Van Hove singularity of the optical transition between two parallel bands in Bernal-stacked bilayer graphene.[1a] In contrast, the reflection spectrum of 0-30 bilayer graphene has no dip feature in the mid-infrared range (Figure 2h), which reflects the decoupled nature of the two layers at low energy.[1a] In this research 15 0-0 bilayer graphene domains and 15 0-30 bilayer graphene domains were investigated by FT-IR spectroscopy and the results were consistent with those shown in Figure 2g–h. The transport behaviors of bilayer and trilayer graphene pyramids were also investigated (Figure S9) in this research. The calculated carrier (hole) mobility of 0-0 bilayer (Bernal-stacked) graphene is about 5000 $cm^2 V^{-1} s^{-1}$ at room temperature on SiO_2/Si substrates, significantly better than that of polycrystalline Bernal-stacked bilayer graphene,[14] indicating the high-quality of as-made graphene single crystals. In addition, N-doped single-crystal bilayer graphene was synthesized by introducing ammonia (Figure S10), providing more potential for further studies in electronics, optics, and thermal conduction of such materials.

An important question is, why are the interlayer rotations in the graphene pyramids almost exclusively either 0° or 30°? The 0° Bernal stacking is not a surprise, since it also dominates in graphite.[6] This is due to the Van der Waals interlayer interaction, which has an energy minimum at 0°, that is, the Bernal stacking configuration. The 30° orientation barely appears in graphite as it is incommensurate stacking. However, our research shows that, the 30° orientation is one of the two preferences in graphene pyramids. This surprising fact is explained below.

We first discuss the possibility that the rotations are induced by the interactions between graphene layers (graphene | graphene), or graphene and Cu substrate (graphene | Cu(111)) surface. The Cu foil used here is mainly composed of (111) surfaces, as shown in Figure S11, by forming the coincidence site lattice (CSL).[15] The CSL is a superlattice composed of two lattices which are mutually rotated but have some atoms coinciding in the same in-plane location. For each CSL angle, there is a Σ which represents the ratio between the number of the atoms in the CSL unit cell and the primitive cell of the component lattice. Typically a smaller Σ corresponds to a lower interface energy, as the density of coincidence atoms which form bonds gets higher. The CSL model has been used to explain the angle preference in crystalline interfaces such as grain boundaries and epitaxial crystals with strong adhesion. In our system, the Cu(111) surface has lattice parameter close to that of graphene (about 4% difference), so the graphene | graphene interface and the graphene | Cu(111) surface share the same type of CSL. The CSL angles and corresponding Σs are plotted in Figure S12. The four lowest Σ and their corresponding angles are: $\Sigma = 1$, 0°; $\Sigma = 7$, 21.8°; $\Sigma = 13$, 27.8°, and $\Sigma = 19$, 13.2°. According to the CSL model, the 21.8° should be preferred as it has the smallest Σ besides the perfect match. However, we do not find such a preference in the experiments (despite some other CSL angles are occasionally found, such as 13° between pyramids in Figure S1). We further calculate the CSL interface energy (as defined in the Supporting Information) for both graphene | graphene and graphene | Cu(111) surface, at different angles, as shown in Figure S12. In both cases, the interface energy shows a minimum at 0°, but similar values for other CSL angles. No preference is found at nearly 30°, in disagreement with the experiments. The graphene | Cu(111) surface interaction was also studied theoretically by Zhang et al.,[16] who do not find 30° preference either. It is interesting to note that the computed energies do not follow the trend predicted by the CSL. It can be attributed to weak dispersive interaction in the interface of our system, compared with strong bonding between atoms in the grain boundary or conventional epitaxial interface where CSL is more applicable. Overall, the above analyses indicate that the interactions between graphene layers or graphene | Cu(111) surface are unlikely to be the major driving force to induce the angle preference in our experiments.

Though the energetics of the grown crystal cannot solve the 30° puzzle, it is well-known that many structural properties are determined at the beginning of crystal growth, that is, nucleation stage. The experimental fact that the graphene pyramids are almost concentric suggests that they share the same nucleation site. For electrochemically polished and annealed Cu, impurities and sharp wrinkles have been

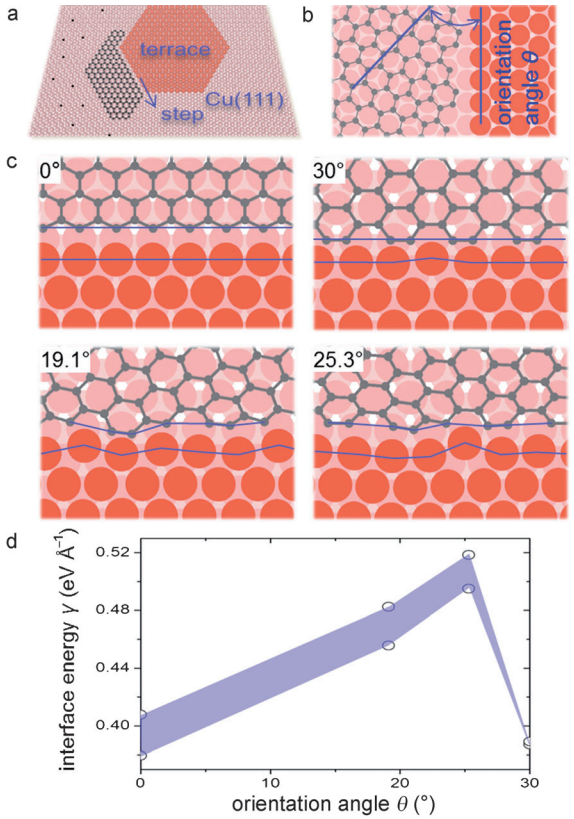

Figure 3. a) Graphene nucleation on the Cu surface. C: black, Cu: red. The topmost Cu layer is highlighted in bold color. b) The orientation angle between graphene and Cu(111) surface. c) The relaxed graphene | Cu step interface structures for different orientation angles. d) The interface energy [defined in Eq. (S1)] as a function of the orientation angle. The two data points at the same orientation angle represent the computational accuracy, because of different strain levels of periodic cell size (either using the Cu or graphene lattice parameter; see details in the Supporting Information).

The above mechanism was quantified by first-principle calculations. The computational details can be found in the Supporting Information. Figure 3c shows the atomic structure of graphene | Cu step interface. Clearly, for 0° (ZZ) and 30° (AC) interfaces, both the graphene edge and Cu step remain almost intactly straight. However, at 19.1° or 25.3°, the Cu step is distorted, and the graphene edge is highly buckled in the surface normal direction, suggesting an unstable interface. Figure 3d confirms that the interface energy [defined in Eq. (S1)] has two local minima at 0° and 30°. Therefore, the graphene | Cu step interface has two preferred orientations: 0° and 30°.

The energy preference for 0° and 30° is also manifested in the electronic structure. Figure 4 shows the charge density difference between the graphene–Cu system and the isolated

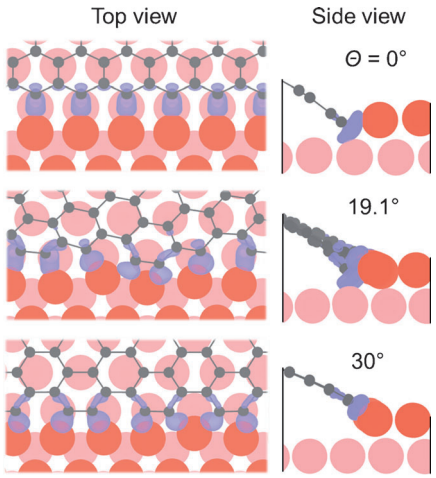

Figure 4. Isosurfaces (in blue) of electron density accumulation upon forming the graphene | Cu step interface. For clarity, only two Cu layers are displayed.

removed (Figure S13), leaving the Cu steps (Figure 3a) as major nucleation sites,[17,18] since they provide low-energy sites for C atoms.[17,19] The steps on the Cu(111) surface are microscopically straight with closest-packed atoms (Figure 3b), as the most stable configuration.[17,19] During nucleation, a graphene | Cu step interface is formed (Figure 3b). The strong interface bonding determines the graphene orientation with respect to Cu(111),[16] and subsequently leads to the mutual orientations between graphene layers in the same pyramid as they nucleate from the same site. Therefore, the energy-preferred graphene | Cu step interface would lead to preferred orientation between graphene and Cu, and eventually result in preferred orientation between graphene layers. The optimal graphene | Cu step interface should be formed by atomically straight graphene edges, because they could efficiently contact the step atoms and saturate their dangling bonds. Among all the orientations, the 0° and 30° orientations render straight zigzag (ZZ) and armchair (AC) graphene edges, respectively. Other edges have rough shapes with alternating straight segments and kinks,[20] which should lead to high-energy interfaces.

graphene and Cu. The electron density accumulation is observed at the interface, suggesting a partially covalent bonding feature of graphene | Cu step interface. It also shows that the ZZ and AC edges have different binding sites. The AC edge (30°) is only bound with Cu step atoms, while the ZZ edge (0°) is also bound with the Cu layer underneath. The extra coordination of the ZZ edge with Cu helps stabilize the interface. For other angles, the graphene edges are combinations of ZZ and AC segments.[20] Their difference in the binding sites distorts the graphene | Cu step interface (19.1° in Figure 4), and gives rise to the high interface energy.

During the CVD growth, the graphene sheet could grow across the Cu step where it originally nucleated,[18] by addition of surface or subsurface diffusing C atoms to the interface. After that, the graphene edge extends, without being "pinned" by the Cu step. Therefore, the Cu steps are re-exposed and serve as the nucleation sites for a second graphene layer. A detailed description on the nucleation of multilayer graphene can be found in the Supporting Information. The new layer again has preference for 0° and 30° with respect to the Cu surface. Since the graphene layers in the same pyramid nucleate from the same site that serves as

a common reference, their mutual rotations should also have the preference for 0° and 30°. Eventually, graphene pyramids grow on clean Cu, with the component layers mutually rotated by either 0° or 30°.

In summary, we report the CVD synthesis of about 100 μm hexagonal bi- and trilayer graphene single crystals on pretreated Cu foils. The as-made graphene domains have almost exclusively either Bernal stacking (0°) or anomalous 30° interlayer rotations. The rotations originate from the graphene nucleation at the Cu step, which is supported by first-principle calculations. The as-made graphene domains were isolated from Cu surfaces and transferred onto silica wafers or trench-patterned silica, enabling the further studies of their thickness- and orientation-dependent electronics and optoelectronics.

Received: July 19, 2013
Published online: January 22, 2014

Keywords: first-principle calculations · graphene · growth mechanism · single crystals · surface chemistry

[1] a) F. Wang, Y. Zhang, C. Tian, C. Girit, A. Zettl, M. Crommie, Y. R. Shen, *Science* **2008**, *320*, 206 – 209; b) A. K. Geim, K. S. Novoselov, *Nat. Mater.* **2007**, *6*, 183 – 191; c) Y. Zhang, T. T. Tang, C. Girit, Z. Hao, M. C. Martin, A. Zettl, M. F. Crommie, Y. R. Shen, F. Wang, *Nature* **2009**, *459*, 820 – 823.

[2] a) A. Reina, X. Jia, J. Ho, D. Nezich, H. Son, V. Bulovic, M. S. Dresselhaus, J. Kong, *Nano Lett.* **2009**, *9*, 30 – 35; b) K. S. Kim, Y. Zhao, H. Jang, S. Y. Lee, J. M. Kim, K. S. Kim, J. H. Ahn, P. Kim, J. Y. Choi, B. H. Hong, *Nature* **2009**, *457*, 706 – 710; c) X. S. Li, W. W. Cai, J. An, S. Kim, J. Nah, D. Yang, R. Piner, A. Velamakanni, I. Jung, E. Tutuc, S. K. Banerjee, L. Colombo, R. S. Ruoff, *Science* **2009**, *324*, 1312 – 1314.

[3] a) P. Y. Huang, C. S. Ruiz-Vargas, A. M. van der Zande, W. S. Whitney, M. P. Levendorf, J. W. Kevek, S. Garg, J. S. Alden, C. J. Hustedt, Y. Zhu, J. Park, P. L. McEuen, D. A. Muller, *Nature* **2011**, *469*, 389 – 392; b) Q. K. Yu, L. A. Jauregui, W. Wu, R. Colby, J. Tian, Z. Su, H. Cao, Z. Liu, D. Pandey, D, Wei, T. F. Chung, P. Peng, N. P. Guisinger, E. A. Stach, J. Bao, S. S. Pei, Y. P. Chen, *Nat. Mater.* **2011**, *10*, 443 – 449.

[4] a) Z. Yan, J. Lin, Z. Peng, Z. Sun, Y, Zhu, L. Li, C. Xiang, E. L. Samuel, C. Kittrell, J. M. Tour, *ACS Nano* **2012**, *6*, 9110 – 9117; b) L.Gao, W. Ren, H. Xu, L. Jin, Z. Wang, T. Ma, L. P. Ma, Z. Zhang, Q. Fu, L. M. Peng, X. Bao, H. M. Cheng, *Nat. Commun.* **2013**, DOI: 10.1038/ncomms1702; c) X. S. Li, C. W. Magnuson, A. Venugopal, R. M. Tromp, J. B. Hannon, E. M. Vogel, L. Colombo, R. S. Ruoff, *J. Am. Chem. Soc.* **2011**, *133*, 2816 – 2819.

[5] a) X. Zou, J. Shang, J. Leaw, Z. Luo, L. Luo, C. Laovorakiat, L. Cheng, S. A. Cheong, H. Su, J. X. Zhu, Y. Liu, K. P. Loh, A. H. C. Neto, T. Yu, E. E. M. Chia, *Phys. Rev. Lett.* **2013**, *110*, 067401; b) Y. Kim, H. Yun, S. G. Nam, M. Son, D. S. Lee, D. C. Kim, S. Seo, H. C. Choi, H. J. Lee, S. W. Lee, J. S. Kim, *Phys. Rev. Lett.* **2013**, *110*, 096602; c) Y. Wang, Z. Ni, L. Liu, Y. Liu, C. Cong, T. Yu, X. Wang, D. Shen, Z. Shen, *ACS Nano* **2010**, *4*, 4074 – 4080; d) L. Zhang, Y. Zhang, J. Camacho, M. Khodas, I. Zaliznyak, *Nat. Phys.* **2011**, *7*, 953 – 957.

[6] M. S. Dresselhaus, G. Dresselhaus, K. Sugihara, I. L. Spain, H. A. Goldberg, *Graphite Fibers and Filaments*, Springer, Berlin, **1988**.

[7] Y. Shibuta, J. A. Elliott, *Chem. Phys. Lett.* **2011**, *512*, 146 – 150.

[8] W. Fang, A. L. Hsu, R. Caudillo, Y. Song, A. G. Birdwell, E. Zakar, M. Kalbac, M. Dubey, T. Palacios, M. S. Dresselhaus, P. T. Araujo, J. Kong, *Nano Lett.* **2013**, *13*, 1541 – 1548.

[9] a) K. I. Bolotin, K. J. Sikes, Z. Jiang, M. Klima, G. Fudenberg, J. Hone, P. Kim, H. L. Stormer, *Solid State Commun.* **2008**, *146*, 351 – 355; b) A. A. Balandin, S. Ghosh, W. Bao, I. Calizo, D. Teweldebrhan, F. Miao, C. N. Lau, *Nano Lett.* **2013**, *13*, 902 – 907.

[10] L. M. Malard, M. A. Pimenta, G. Dresselhaus, M. S. Dresselhaus, *Phys. Rep.* **2009**, *473*, 51 – 87.

[11] Y. Hernandez, V. Nicolosi, M. Lotya, F. M. Blighe, Z. Sun, S. De, I. T. McGovern, B. Holland, M. Byrne, Y. K. Gun'Ko, J. J. Boland, P. Niraj, G. Duesberg, S. Krishnamurthy, R. Goodhue, J. Hutchison, V. Scardaci, A. C. Ferrari, J. N. Coleman, *Nat. Nanotechnol.* **2008**, *3*, 563 – 568.

[12] K. Kim, S. Coh, L. Z. Tan, W. Regan, J. M. Yuk, E. Chatterjee, M. F. Crommie, M. L. Cohen, S. T. Louie, A. Zettl, *Phys. Rev. Lett.* **2012**, *108*, 246103.

[13] J. C. Meyer, A. K. Geim, M. I. Katsnelson, K. S. Novoselov, T. J. Booth, S. Roth, *Nature* **2006**, *439-444*, 60 – 63.

[14] a) K. Yan, H. Peng, Y. Zhou, H. Li, Z. Liu, *Nano Lett.* **2011**, *11*, 1106 – 1110; b) S. Lee, K. Lee, Z. Zhong, *Nano Lett.* **2010**, *10*, 4702 – 4707.

[15] a) W. Bollmann, *Crystal Defects and Crystalline Interfaces*, Springer, Berlin, **1970**; b) D. H. Warrington, *J. Phys. (Paris), Colloq.* **1975**, *36*, C4-87 – C4-95.

[16] X. Zhang, Z. Xu, L. Hui, J. Xin, F. Ding, *J. Phys. Chem. Lett.* **2012**, *3*, 2822 – 2827.

[17] a) J. Gao, J. Yip, J. Zhao, B. I. Yakobson, F. Ding, *J. Am. Chem. Soc.* **2011**, *133*, 5009 – 5015; b) V. I. Artyukhov, Y. Liu, B. I. Yakobson, *Proc. Natl. Acad. Sci. USA* **2012**, *109*, 15136 – 15140.

[18] a) L. Gao, J. R. Guest, N. P. Guisinger, *Nano Lett.* **2010**, *10*, 3512 – 3516; b) G. H. Han, F. Günes, J. J. Bae, E. S. Kim, S. J. Chae, H.-J. Shin, J.-Y. Choi, D. Pribat, Y. H. Lee, *Nano Lett.* **2011**, *11*, 4144 – 4148.

[19] S. Saadi, F. Abild-Pedersen, S. Helveg, J. Sehested, B. Hinnemann, C. C. Appel, J. K. Nørskov, *J. Phys. Chem. C* **2010**, *114*, 11221 – 11227.

[20] Y. Liu, A. Dobrinsky, B. I. Yakobson, *Phys. Rev. Lett.* **2010**, *105*, 235502.

